The Origin of Outflows in Evolved Stars
Proceedings IAU Symposium No. 366, 2022
L. Decin, A. Zijlstra & C. Gielen, eds
doi:10.1017/S1743921322000898

Morpho-kinematics around cool evolved stars Unveiling the underlying companion

I. El Mellah[1], J. Bolte[2], L. Decin[2], W. Homan[3] and R. Keppens[4]

[1]Institut de Planétologie et d'Astrophysique de Grenoble, UGA-CNRS, rue de la Piscine, 38400
email: ileyk.elmellah@univ-grenoble-alpes.fr

[2]Institute of Astronomy, KU Leuven, Celestijnenlaan 200D, 3001 Leuven, Belgium

[3]Institut d'Astronomie et d'Astrophysique, campus Plaine, Boulevard du Triomphe, Brussels, Belgium

[4]Centre for mathematical Plasma-Astrophysics, Celestijnenlaan 200B, 3001 Leuven, Belgium

Abstract. Because they lose tremendous amounts of mass, cool evolved stars are major sources of dust and molecules for the interstellar medium. Spectro-imaging of the dust-driven winds around these stars has enabled us to identify recurring nonspherical patterns (e.g. spirals, arcs, compressed wind). We use radiative-hydrodynamic simulations of dust-driven winds to study the imprints left in the wind by an orbiting stellar or sub-stellar companion. We designed 3D numerical setup to solve the wind dynamics beyond the dust condensation radius and follow the flow up to several hundreds of stellar radii. Non-uniform grids enable us to capture small scale features such as shocks or disks forming around the orbiting object. Depending on its mass and orbital parameters, we reproduced typical non-spherical features such as arcs, spirals, petals and orbital density enhancements, and identified patterns associated to eccentric orbits.

Keywords. stars:evolution - stars:winds,outflows - stars:AGB and post-AGB - methods:numerical - binaries:general

1. Introduction

In the stages following main sequence, mass loss plays a major role in the evolution of the star itself. As the star expands, it cools down but the luminosity remains approximately the same. As a consequence, the effective gravity drops and stellar material can more easily detach from the star. This is the case for red giant and supergiant stars (RSGs) and asymptotic giant branch stars (AGBs). These stars loose mass at rates which peak at 10^{-7}-10^{-5}M$_\odot$/year via a wind whose speed typically ranges from 5 km/s to 20km/s.

The mechanism which brings stellar material in the outermost layers at escape speed is still poorly understood. It hampers our attempts to determine the final fate of stars and thus leading to inaccurate occurrence rates for compact objects. However, wind launching is believed to be made possible by the combined action of convection, pulsations, molecular line absorption and continuum dust opacity (Höfner & Olofsson 2018). In the piston model, which proves to be accurate for AGB stars, the material is lifted by radial pulsations controlled by the κ-mechanism. Internal shocks form and as the temperature decreases, molecules form and condensate into dust grains. The latter absorb the continuum stellar spectrum which produces a net outward force due to radiative pressure (Freytag, Liljegren & Höfner 2017). Depending on the chemical content of the dust (carbon-rich or oxygen-rich), the opacity can be more or less high, with important

consequences on the terminal wind speed and on the velocity profile. Alternatively, for RSGs, Kee et al. (2021) developed a model where turbulence pressure in the atmosphere provides enough outward momentum without the need for dust opacity.

On the other hand, stellar multiplicity has been recognized as a ubiquitous feature: stars seldom live an effectively single life. Due to their low speed, dust-driven winds can lead to significant mass transfer to the orbiting companion in binary systems where the donor star (the primary) has evolved beyond the main sequence. This mechanism is thought to be responsible for the peculiar chemical composition of certain stars (e.g. CEMP stars, Barium stars, blue stragglers). During this IAU Symposium, the evolutionary importance of chemical contamination was highlighted by Morgan Deal (for Lithium depletion) and Anke Andersen (for very metal-poor stars in the inner regions of the Milky Way). Through its gravitational influence on the primary and on the wind itself, the companion (the secondary) would also leave imprints in the fraction of the wind which escapes the binary. The nature of these marks depends on the companion mass, on its orbit and on the chemical composition of the circumbinary envelope.

The advent of a new generation of high spatial and spectral resolution instruments has ushered in a gold rush to understand mass loss of cool evolved stars. In the optical, the Hubble Space Telescope monitors dust emission while the Herschel Space Observatory and the (sub)millimeter interferometer ALMA capture the emission associated to molecular rotational and vibrational transitions. Through spectro-imaging, they grant us access to the 3D morpho-kinematics of the wind with multi-channel molecular line emission maps. They have not only revealed the complexity of the astrochemistry at work but also identified nonspherical features in these cool winds. The ALMA large program ATOMIUM has identified recurrent axisymmetric patterns like spirals, arcs or petal-like patterns (Decin *et al.* 2020). Although alternative scenarios exist, these features have been ascribed to the presence of an underlying stellar or sub-stellar companion, too dim to be directly detected.

2. Model

2.1. *Wind launching*

We developed a simplified prescription for the launching of the wind from an isolated cool star which enables us to differentiate between carbon-rich and oxygen-rich outflows. The wind from carbon-rich AGB stars reaches its terminal speed within a few dust condensation radii at most. On the contrary, for oxygen-rich outflows, the acceleration is much more progressive due to the lower opacity of the dust grains formed. We solve the 1D steady spherical equation of motion, neglecting the thermal pressure:

$$v\frac{dv}{dr} = -\frac{1}{r^2} + \frac{\Gamma}{r^2}\kappa\left(r\right) \tag{2.1}$$

where length and speed were normalized to the dust condensation radius and the escape speed at the dust condensation radius respectively. Γ is a constant ratio of luminosity similar to the Eddington parameter, but with a reference opacity κ_0 defined as:

$$\Gamma = \frac{\kappa_0 L_*}{4\pi G M_* c} \tag{2.2}$$

where M_* is the mass of the donor star, L_* is its luminosity, c is the speed of light and G is the gravitational constant. The effective opacity κ_0 stands for the normalization of the dust opacity but it also represents the coupling between the dust and the gas. It is typically much higher than the dust-free molecular gas opacity.

https://doi.org/10.1017/S1743921322000898 Published online by Cambridge University Press

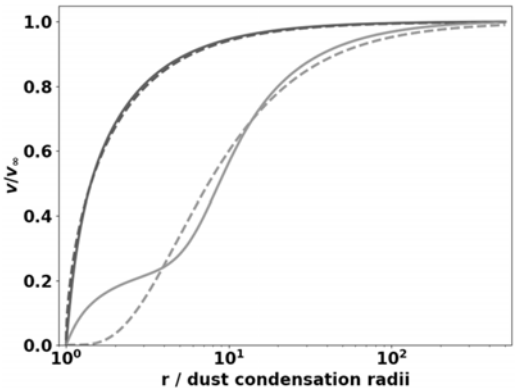

Figure 1. Velocity profiles normalized to escape speed v_∞ numerically integrated (solid lines) and fitted by *beta*-velocity profiles (dashed lines) for carbon and oxygen-rich outflows (upper and lower curves respectively).

To determine the dust opacity profile as a function of distance to the star, we connect it to the local equilibrium temperature T of the star given by:

$$T(r) = \frac{T_*}{2}\left[1 - \sqrt{1 - (R_*/r)^2}\right]^{1/4} \tag{2.3}$$

where T_* is the stellar effective temperature and R_* is the stellar radius. Bowen (1988) suggested the following dimensionless opacity profile to mimic the dust growth in carbon-rich outflows:

$$\kappa = \frac{1}{1 + \exp\left(T - T_c\right)/\Delta T}, \tag{2.4}$$

with T_c the dust condensation temperature and ΔT a range of temperature where the grains grow. For realistic values for stellar parameters and opacity of carbon-rich winds ($\kappa_0 \sim 5{-}10$ g·cm^{-2}), we obtain the solid upper line shown in Figure 1, very well fitted by a β-law with $\beta \sim 0.6$ (dashed upper line).

For oxygen-rich outflows, we assume that a two-stages acceleration mostly driven by two dust species, 1 and 2. Dust species 1 condensates at a higher temperature ($T_{c,1} > T_{c,2}$) but its opacity is not sufficient to bring the material to escape speed. Instead, it lifts the material up to distances where dust species 2 condensates and drives a proper wind. We obtained the solid lower velocity profile in Figure 1 which can be fitted by a β-law with $\beta \sim 5$ (dashed lower line).

2.2. *Numerical setup*

We inject the 1D acceleration profiles derived in the previous section into a 3D numerical setup centered on the donor star. We used the `MPI-AMRVAC` code (Xia et al. 2017) in order to solve the equations of hydrodynamics on a spherical grid radially stretched (El Mellah et al. 2015). For circular orbits, we work in the co-rotating frame such as the source terms are those induced by the non-inertial forces, the gravitational pull from the two bodies and the radiative pressure due to continuum opacity on dust grains. Instead of solving the equation of energy, we assume that the expansion of the wind is adiabatic with a polytropic index of 1.3. With this value, we match the observed temperature profiles $T \propto r^{-0.6}$. With 4 levels of adaptive mesh refinement, the effective resolution of these simulations is 1,280×512×1,024. The 3 dimensionless parameters of our model are:

https://doi.org/10.1017/S1743921322000898 Published online by Cambridge University Press

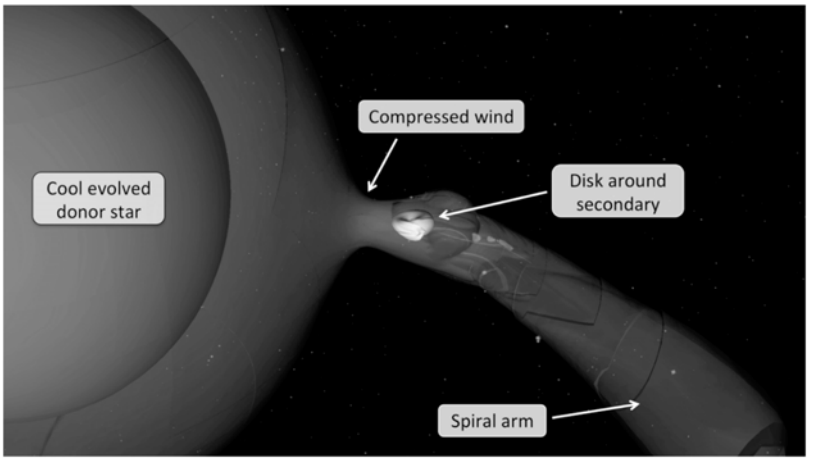

Figure 2. Structure of the flow at the orbital scale. Iso-density surfaces are represented.

(1) the ratio η of the terminal wind speed v_∞ to the orbital speed $a\Omega$, with a the orbital separation and Ω the angular orbital speed.
(2) the mass ratio q (primary to secondary).
(3) the filling factor f (ratio of dust condensation radius to Roche lobe radius).

and the donor star can be either carbon or oxygen-rich. We explored 70 different configurations whose parameters can be found in El Mellah et al. (2020).

3. Results

3.1. *Wind-captured disks*

Although the dust condensation radius is much smaller than the Roche lobe radius of the primary ($f \ll 1$), we do observe features reminiscent of Roche lobe overflow (RLOF) mass transfer (see Figure 2). The wind is beamed in the orbital plane and a tidal arm develops towards the secondary. A nozzle appears near the inner Lagrangian point and a tidal arm forms in the wake of the secondary. In some cases, the flow even gains enough angular momentum to form a wind-captured disk around the secondary, similar to what is observed in high-mass X-ray binaries (El Mellah et al. 2018). These properties are characteristic of the wind-RLOF mechanism highlighted by Mohamed et al. (2007) where the outflow is significantly affected by the presence of the secondary. In our simulations, it typically corresponds to low values of η, and, to a lesser extent, to high values of q and f. Because acceleration is more progressive for oxygen-rich outflows, they are more prone to undergo this mass transfer mechanism. A contrario, winds which quickly reach a terminal speed much higher than the orbital speed are more radial and less affected by the presence of the secondary.

This wind-RLOF mechanism is also associated to an increasing fraction of the wind being accreted by the secondary, which leads to a slower widening of the orbit compared to a pure mass loss configuration. For sufficiently low mass companion (e.g. a massive planet) and/or for sufficiently high fraction of the wind captured, the orbit can even shrink at a quick pace, which leads to an enhanced fraction of the wind being captured and a runaway spiral in.

https://doi.org/10.1017/S1743921322000898 Published online by Cambridge University Press

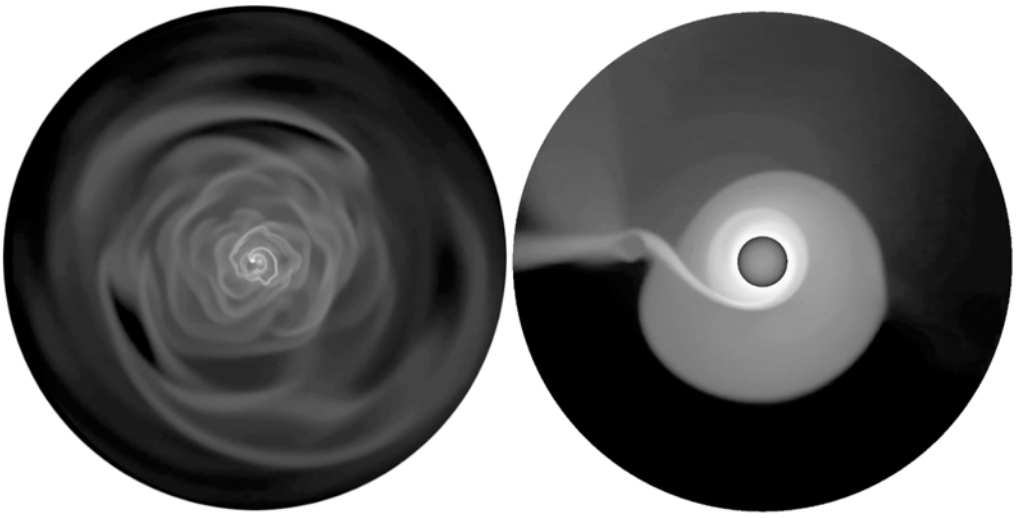

Figure 3. (Left panel) Global flow morphology for a wind computed for a companion on a circular orbit around an O-rich star. In the center, the two bodies are visible. Petal-like patterns are imprinted in the circumbinary envelope up to distances much larger than the orbital separation. (Right panel) Slice in the orbital plane of the wind density with the donor star in the center and the companion at apoastron.

3.2. *Morpho-kinematics of the circumbinary envelope*

At a broader scale, we reproduce the nonspherical features observed like spirals, arcs, petal-like patterns (Figure 3, left panel) and equatorial density enhancement. The latter has been shown by Decin et al. (2019) to be responsible for the overestimated mass loss rates derived when overlooking this compression of the wind. The spiral shocks develop due to the wobbling of the primary induced by the secondary. In these 3D simulations, we can also study the impact of the line-of-sight. Spiral shocks appear as concentric arcs when seen edge-on while the petal-like patterns emerge when the terminal wind speed is of the order of the orbital speed, leading to a marginally unbound outflow.

In order to confront these simulations to observations, we are currently extracting from these simulations synthetic molecular line emission maps. The density and temperature maps can be used to compute 1D chemical abundance profiles (Van de Sande et al. 2019). Combined with the velocity maps, we can use a radiative transfer code to obtain from each cell the Doppler-shifted molecular line emission for each frequency bin.

3.3. *Eccentric orbits: companion-driven winds*

For eccentric orbits, we reach within a few orbital periods a regime where the morphology of the outflow is set by the orbital phase. We ran a simulation with an eccentricity of 0.5 and a $f = 1$ at periastron (Figure 3, right panel). In this case, we found that the gravitational slingshot induced by the passage of the secondary at periastron drives an increase in the instantaneous mass loss rate. If confirmed, a correlation between the mass loss rate and the eccentricity of the companion's orbit would point in favor of a boosting mechanism for wind launching and new types of companion-stimulated winds.

4. Conclusions

We showed that an orbiting companion could reproduce most nonspherical features observed in the circumbinary envelope of cool stars. The main parameter driving the

https://doi.org/10.1017/S1743921322000898 Published online by Cambridge University Press

wind dynamics is the ratio η of the terminal wind speed to the orbital speed. As η decreases toward 1, the pitch angle of the spiral shock decreases. For $\eta \lesssim 1$, the spiral fragments into arcs which are intermittently ejected by incoming material. It produces a petal-like pattern which is reminiscent, when observed face-on, of the morphology of the C-rich AGB star CW Leo for instance.

Acknowledgments

The author wishes to thank the ATOMIUM ALMA Large Programme collaboration (2018.1.00659, PI. L. Decin) for the observational consequences of the present analysis. IEM has received funding from the Research Foundation Flanders (FWO) and the European Union's Horizon 2020 research and innovation program under the Marie Skłodowska-Curie grant agreement No 665501. The simulations were conducted on the Tier-1 VSC (Flemish Supercomputer Center funded by Hercules foundation and Flemish government).

References

Bowen, G. 1988, *ApJ*, 329, 9, 299

Decin, L., Montargès, M., Richards, A. M.S., Gottlieb, C. A., Homan, W., McDonald, I., El Mellah, I., Danilovich, T., Wallström, S. H.J., Zijlstra, A., Baudry, A., Bolte, J., Cannon, E., De Beck, E., De Ceuster, F., de Koter, A., De Ridder, J., Etoka, S., Gobrecht, D., Gray, M., Herpin, F., Jeste, M., Lagadec, E., Kervella, P., Khouri, T., Menten, K., Millar, T. J., Müller, H. S.P., Plane, J. M.C., Sahai, R., Sana, H., Van de Sande, M., Waters, L. B.F.M., Wong, K. T., Yates, J. 2020, *Science*, 369 , 6509, 1497

Decin, L., Homan, W., Danilovich, T., de Koter, A., Engels, D., Waters, L.B.F.M., Muller, S., Gielen, C., García-Hernández, D. A., Stancliffe, R. J., Van de Sande, M., Molenberghs, G., Kerschbaum, F., Zijlstra, A. A., El Mellah, I. 2019, *Nature Astronomy*, 3, 5, 408

El Mellah, I. and Casse, F. 2015, *MNRAS*, 454, 3, 2657

El Mellah, I., Sander, A. A. C., Sundqvist, J. O., Keppens, R. 2019, *A&A*, 622, A189

El Mellah, I. et al. 2020, *A&A*, 637, A91

Freytag, B., Liljegren, S., Höfner, S. 2017, *A&A*, 600, A137

Höfner S., Olofsson H. 2018, *AAR*, 26, 1

Kee, N. D., Sundqvist, J. O., Decin, L., De Koter, A., Sana, H. 2021, *A&A*, 646, A180

Mohamed, S. and Podsiadlowski, P. 2007, PhD Manuscript

Van de Sande, M., Walsh, C., Mangan, T. P., Decin, L. 2019, *MNRAS*, 490, 2, 2023

Xia, C., Teunissen, J., El Mellah, I., Chané, E., Keppens, R. 2017, *ApJS*, 234, 2, 30